Research Article

Mass-Based Hybrid Nanofluid Model for Thermal Radiation Analysis of MHD Flow over a Wedge Embedded in Porous Medium

Sushila Choudhary [1], **Vijendra Kumar Jarwal,**[1] **Prasun Choudhary** [1], **K. Loganathan** [2], **and Balachandra Pattanaik** [3,4]

[1]*Department of Mathematics, University of Rajasthan, Jaipur 302004, Rajasthan, India*
[2]*Department of Mathematics and Statistics, Manipal University Jaipur, Jaipur 303007, India*
[3]*College of Engineering and Technology, Wollega University, Nekemte, Ethiopia*
[4]*Saveetha School of Engineering, Saveetha Institute of Medical and Technical Sciences, Chennai, India*

Correspondence should be addressed to K. Loganathan; loganathankaruppusamy304@gmail.com and Balachandra Pattanaik; balapk1971@gmail.com

This study addresses the intricate interplay of magnetohydrodynamics (MHD), thermal radiation, and porous media effects, which are crucial in numerous engineering applications, including aerospace, energy systems, and environmental processes. The development of a mass-based hybrid nanofluid model signifies a novel approach, potentially yielding more accurate predictions and insights into the thermal behavior of fluids in diverse scenarios. Thus, the current research explores the heat transfer characteristics of a unique nanofluid known as TiO_2 (titania)-CuO (copper oxide)/H_2O (water) hybrid nanofluid. This nanofluid flows past a static or moving wedge considering the impact of thermal radiation and magnetic field in the appearance of porous medium. To calculate the effective thermophysical attributions of the hybrid (TiO_2-CuO) nanofluid, a mass-based strategy is employed. This approach involves analyzing the masses of both the first and second nanoparticles, along with the mass of the base fluid, as essential input parameters. The proposed mathematical model is modified to a dimensionless form by applying similarity transformations. The numerical solution is obtained by utilizing the bvp4c built-in function within the MATLAB environment. Graphs illustrate the influence of various parameters on temperature and velocity trends, including the magnetic field parameter and heat absorption/generation parameter as well as the thermal radiation parameter. It is noted that along with the enhancement in the values of parameters related to porous medium or magnetic field, the velocity of the hybrid nanofluid improves. This occurs when the moving wedge parameter's value is below 1. Conversely, when the moving wedge parameter's value exceeds 1, the velocity of the hybrid nanofluid decreases. The shape factor is more effective in the temperature profile for developed inputs of heat absorption/generation parameter. A juxtaposition of enhancement in heat transfer rate due to nanofluid (TiO_2/H_2O) and hybrid nanofluid (TiO_2-CuO/H_2O) is likewise presented. The main outcome indicates that the hybrid nanofluid exhibits superior thermal conductivity relative to the conventional nanofluid.

1. Introduction

Nanofluid is a blend of fundamental fluids (mainly liquids) such as ethylene glycol, water, and engine oil, and nanometer-sized solid particles (Ag, Cu, and Al), which was first introduced by Choi [1]. He observed that the thermal capability of traditional fluids was enhanced when nanoparticles were scattered into the above-mentioned base fluids. Due to the stability and reactivity of metallic nanoparticles, their uses are limited in the field of nanofluid applications. Viewing the features of nonmetallic and metallic nanoparticles, it can be observed that the thermophysical properties of a nanofluid, which is a composition of Al_2O_3 nanoparticles in fundamental fluid, can be enhanced

by adding metal nanoparticles in it [2]. Many researchers use oxide nanoparticles to boost the thermal conductivity of working base fluid which signifies that oxides are a good substitution for metal nanoparticles and carbon nanoparticles. Nanofluids are widely used in nanotechnologies due to its several order larger thermal conductivities than traditional fluids such as ethylene glycol, water, and different oils. Due to high thermal conductivity at low cost, long-term stability, and good fluidity, nanofluids are also utilized in different industrial and engineering areas. Nayak et al. [3] have shown some experimental results for thermal expansion behavior of several nanofluids as application of heat removal systems considering various nanoparticles such as Al_2O_3, CuO, SiO_2, and TiO_2. Dinarvand and Pop [4] evaluated heat transfer of an electrically conductive nanofluid (copper/water) with the effect of cross-magnetic field applying Tiwari–Das nanofluid model over a revolving cone. There is growing interest in the advanced level of nanofluid called "hybrid nanofluid," which is produced by combining distinct kinds of nanoparticles within an already-existing nanofluid. Hybrid nanofluid has high effective thermal conductivity when it is compared to mono nanofluids (a nanofluid with one type of nanoparticles). Due to the excellent characteristics of hybrid nanofluids, they are helpful for many applications, including electronic cooling, heat interchangers, lubrication, solar heating, refrigeration, nuclear system cooling, defense, biomedical, drug reduction, and space aircraft. Using both single and dual nanoadditives, Jana et al. [5] looked into improving fluid thermal conductivity. Baghbanzadeh et al. [6] analyzed the consequences of hybrid nanostructures such as multiwall carbon nanotube and silica nanospheres on thermal conductivity of related basic fluid. Nuim Labib et al. [7] explored the impact of convective heat on two different base fluids with mixing of Al_2O_3 as nanoparticles. Numerical investigation is carried out on forced convection of pure-water-based nanofluid (Al_2O_3/H_2O) and hybrid nanofluid ($Al_2O_3–Cu/H_2O$) in turbulent regime by Takabi and Shokouhmand [2]. Sunder et al. [8] have published a research article that focuses on thermal attributes, heat transfer features, and virtues of the friction factor of hybrid nanofluid. In the appearance of chemical reaction and thermal radiation, Hayat and Nadeem [9] pointed out that the nanofluid with more than one type of nanoparticles has a rich heat transfer rate relative to single particle nanofluid. Garia et al. [10] and Jat and Sharma [11] have studied nanofluids over different surfaces to analyze fluid flow and heat transfer phenomena. There are several studies (both theoretical and experimental) available on hybrid nanofluids to explain their applicability over simple nanofluids. To understand thermal performance of hybrid nanofluid (Al_2O_3-Cu/water), Momin [12] and Suresh et al. [13] have represented some useful experimental data. For the purpose of studying the mixed convection movement of hybrid nanofluid in an upward-facing microchannel, Xu and Sun [14] offered a comprehensive hybrid nanofluid model with numerous types of nanoparticles lying in a fundamental fluid. Sagheer et al. [15] investigated how nonuniform heat sources/sinks affect the flow of an upper-convected Maxwell

nanofluid along a stretching surface heated by convection. They ensure the accuracy of their numerical findings by utilizing the shooting technique, supplemented with the bvp4c MATLAB function. Shah et al. [16] conducted a detailed numerical analysis examining the flow of upper-convected Maxwell (UCM) nanofluids in 3-D, which were induced by a stretching surface. Their primary objective was to explore the influence of nanoparticles on heat and mass transfer within this specific scenario. They developed a model that accounted for thermophoresis and Brownian motion effects to better understand the phenomenon.

Because of its variety of uses in astrophysics, geophysics, and technology during the past few decades, the magnetohydrodynamic (MHD) nanofluid concept has gained more significance. Due to the significant behavior of MHD at high temperature, it attracts tremendous interest from researchers in fields such as reactors, satellites, gas turbines, missiles, and microelectronics. Magnetohydrodynamic (MHD) is a term for the influence of a magnetic field on a moving fluid that was initially examined by Alfvén [17]. Sparrow and Cess [18] conducted a study that delved into the occurrence of natural convection in an electrically conducting fluid when subjected to the influence of a magnetic field. Makinde and Aziz [19] conducted a numerical investigation to examine the behavior of a nanofluid flow within the boundary layer over a stretching sheet subjected to convective boundary conditions. Thermal radiation holds a crucial role in the functioning of space technology equipment, particularly when operating under extremely elevated temperatures. Hady et al. [20] and Pal et al. [21] delved into the examination of the viscous movement and heat transfer in a radiative nanofluid over a sheet that experiences nonlinear stretching or shrinking. Meanwhile, Anwar et al. [22] described the effect of heat generation or absorption on the magnetohydrodynamic (*MHD*) movement of a nanofluid across a porous moving surface, which also involved chemical reactions. The movement of water-based nanofluid involving buoyancy effects and thermal radiation in control of a transverse magnetic field was analyzed by Rashidi et al. [23]. Das et al. [24] explored mixed consequences of Joule heating and viscous dissipation in the context of magnetohydrodynamic slip flow occurring over an inclined plate. Devi and Devi [25] have presented a numerical study, which is focused on the hydromagnetic hybrid nanofluid (Cu and Al_2O_3 as nanoparticles in base fluid water) movement past a spongy and stretchable surface. A numerical analysis is carried out by Kandasamy et al. [26] for the effects of nanoparticle shapes on the MHD flow of nanofluid with thermal radiation over a porous sheet. Ghadikolaei et al. [27] and Sheikholeslami and Shamlooei [28] explored the influence of a generated magnetic field on thermophysical characteristics of hybrid nanofluid and mono nanofluid, with particular consideration given to the impact of the shape factor. Ashorynejad and Shahriari [29] conducted an investigation on the phenomenon of natural convective flow within an open wavy cavity for a hybrid nanofluid, which is composed by mixing of Al_2O_3 and Cu nanoparticles in water while applying a uniform magnetic

field. Choudhary and Jarwal [30] conducted a study exploring the characteristics of *MHD* nanofluid flow, addressing the consequence of thermophoresis, Brownian motion, Navier slip, and convective heating, over an extending sheet. Atif et al. [31] studied how MHD micropolar nanofluid behaves when it flows past a surface that is being stretched. Instead of using traditional models, they used advanced non-Fourier and non-Fick's models to analyze the system in detail. They also looked at various factors such as viscous dissipation, thermal radiation, and Ohmic heating, which were all included in the energy equation. Choudhary and Chand [32] investigated the heat transfer of a magnetohydrodynamic nanofluid movement past a circular cylinder using thermal radiation and Joule heating. Jarwal et al. [33] undertook an investigation aimed at evaluating rise in heat transfer due to flow of two distinct nanofluids, namely, Ag-H_2O and Cu-H_2O. Their analysis took into account the influence of some external factors, including thermal radiation and magnetic field. The findings of their study led them to conclude that Cu-H_2O nanofluid exhibits greater convective heat transfer capabilities than Ag-H_2O nanofluid. Mohana and Rushi Kumar [34] conducted an investigation of the unsteady three-dimensional hybrid nanofluid flow with convective heat transfer past a stretching sheet, employing the Darcy–Forchheimer model. They specifically focused on the study of the behavior of nanofluid made of cadmium telluride and graphite nanoparticles of brick and blade shapes suspended in water. This analysis considered the impact of viscous dissipation and Joule heating on the nanoparticles' behavior in the nanofluid flow. Mohana and Kumar ([35, 36]) delved into an examination of how the shape of nanoparticles influences the hydromagnetic flow of a nanofluid consisting of copper and water, exploring various effects in the process.

Fluid flow with moving wedge called "Falkner–Skan problem," is an important phenomenon which is applied in various engineering applications. Falkner–Skan flow analysis is significant for understanding the behavior of fluid near a solid surface. The Falkner–Skan equations provide solutions for the boundary layer thickness and velocity distribution along a surface, offering valuable insights into the drag forces experienced by objects moving through fluids. This analysis is particularly relevant in aerospace engineering, where minimizing drag is essential for optimizing fuel efficiency and the overall performance of aircraft. Moreover, Falkner–Skan flow plays a pivotal role in diverse applications, ranging from heat exchangers to the design of streamlined vehicles, contributing significantly to the development and improvement of various engineering processes and technologies. For instance, these activities include crafting paper, the process of wire drawing, the art of carpet making, and the shaping of plastic sheets, polymeric sheets, and fiber mats, as well as shaping thin sheets. Velocities related to fluid flow and wedge are proportionate to each other in this phenomenon. Falkner and Skan [37] dealt with the viscous flow in two dimensions across a nearly infinite plate (wedge with zero angles) and numerically solved the governing nonlinear PDEs, which are converted to a self-similar type third-order ODEs known as the Falkner–Skan equations. Ishak et al. [38] presented a theoretical study entitled "Falkner–Skan equation for flow past a moving wedge with suction or injection." Numerous research studies have been conducted to explore various aspects of nanofluid flow over wedges, taking into account different parameters and conditions. Yacob et al. [39] have explored the nature of a boundary layer flow past a stationary or moving wedge, where a wedge is placed within a nanofluid. They performed the numerical analysis of the flow problem with the help of NAG routine DO2HAF and Keller box method. Tamim et al. [40] delved into the study of magnetohydrodynamic mixed convection within the boundary layer of a nanofluid flow. Specifically, their investigation focused on 2-D stagnation point flow over a vertical permeable plate (wedge with 180-degree angles). Nadeem et al. [41] looked into viscous fluid movement with an induced magnetic field over a stationary/moving wedge. Gaffar et al. [42] conducted a study on the topic entitled "Computational modeling and solutions for mixed convection boundary layer flows of nanofluid from a non-isothermal wedge." Sudhagar et al. [43] also explored mixed convection flows with convective boundary conditions. They studied how these conditions influenced heat and mass transfers within a nanofluid. Specifically, their investigation focused on flow over an isothermal vertical wedge that was situated in a porous medium, notable for its non-Darcy behavior. Dinarvand et al. [44] addressed an article to explore behavior of a 2-D boundary layer movement of a hybrid nanofluid (TiO_2-CuO/H_2O) over a stationary or dynamic wedge. Kumaran et al. [45] conducted research that involved analyzing the numerical aspects of a 2-D, incompressible MHD Falkner–Skan flow. This flow pertains to the Carreau nanofluid and was studied over a wedge, plate, and stagnation region of a flat plate. This investigation considered convective boundary conditions and chemical reactions in the process. Bibi and Xu [46] investigated the influence of homogeneous-heterogeneous responses on the movement of magnetohybrid nanofluid within a symmetric channel, while also considering the thermal radiation effect and velocity slip condition. Rawat et al. [47] conducted a comparative analysis of the flow characteristics over a vertical cone and wedge immersed in a Cu-water nanofluid. Their investigation involved employing effective models for thermal conductivity and viscosity. Additionally, they have applied the zero-mass flux condition at the surfaces of both the cone and wedge. The laminar incompressible and electrically conducting magnetohybrid nanofluid movement within an isothermal wedge in combination with Joule heating and viscous heating was identified by Mahanthesh et al. [48]. In their research, Kakar et al. [49] explored fluid flow at the stagnation point of a hybrid nanofluid which is made by different nanoparticles (Al_2O_3 and Cu), with H_2O as the fundamental fluid. They also considered the influence of the melting heat transfer effect while examining the flow past a dynamic wedge. Bhatti et al. [50] discussed the benefits of using magnetic nanoparticles for solar energy applications in the area of heat transfer.

Yaseen et al. [51] extended the Falkner–Skan problem to encompass the effects of nanoparticle aggregation on a stretching or shrinking wedge. Their model incorporates the influence of magnetic field, thermal radiation, and suction/injection effects. Kumar Rawat et al. [52] delved into the flow characteristics of a titania-ethylene glycol nanofluid (TiO_2/EG) over a wedge, taking into account the influence of nanoparticle aggregation. Their study aimed to contribute to the advancement of the Falkner–Skan problem. This analysis incorporated factors such as suction/injection effects, mixed convection, and nonuniform heat source/sink within the flow scenario. Kumar et al. [53] presented a numerical solution to tackle the complex interaction between nonlinear radiation and chemical reactions in an MHD Williamson nanofluid flow around a moving permeable wedge. Their research accounted for factors such as heat generation, Brownian motion, and thermophoretic effects, providing a comprehensive understanding of these intricate phenomena. Bing Kho et al. [54] revealed a numerical simulation of MHD hybrid nanofluid movement considering viscous dissipation and heat radiation over a permeable wedge.

Currently, there is a lack of findings on the heat transfer features of magnetohybrid (TiO_2-CuO/H_2O) nanofluid flow past a stationary/moving wedge, considering thermal radiation and porous medium impacts, using a mass-based computational procedure based on existing literature in the field of nanofluids and hybrid nanofluids. This study aims to fill this gap by analyzing the aforementioned topic, while also examining variations of the size factor on velocity profile and temperature profile. During the investigation, variations in heat transfer rate will be explored, particularly when free stream velocity and moving wedge velocity are in the same path or in the opposite direction. The base fluid and nanoparticles are considered to make a homogeneous working fluid, in which fluid and particles, both are in thermal equilibrium. The Tiwari and Das [55] model is used as a nanofluid model. By utilizing similarity conversion, the governing model, which is in the form of boundary layer equations, is reduced to a dimensionless form. Also, numerical findings are attained by applying the MATLAB built-in function "bvp4c." For bvp4c code validation, the

present problem is also solved using a shooting technique with the Runge–Kutta fourth-order method. Through graphical representations or tabulated data, the study explores the influence of many parameters, including nanoparticle shape factor and mass on velocity profile, temperature profile, and heat transfer characteristics. Code validation results and residual errors are also presented via tables.

In this study, we are investigating an appealing scenario involving an electrically conducting water-based hybrid nanofluid. The considered hybrid nanofluid contains two disjoint nanoparticles, named TiO_2 (titania) and CuO (copper oxide). Our focus lies on a steady 2-D boundary layer flow, whereby the fluid moves past a stationary or moving wedge. The flow characteristics are expected to be laminar, and the nanofluid is treated as incompressible throughout the analysis. The thermal conditions of the fundamental fluid, in this case, water and introduced nanoparticles (TiO_2 and CuO), have been assumed to be in equilibrium, preventing any occurrence of thermal slip between them. To characterize the geometric configuration, we define x-axis as running parallel to the surface of the wedge and the y-axis as oriented normal to it. We apply a magnetic field with variable intensity $B(x)$ directed vertically towards the wedge's surface. Figure 1 shows the physical configuration of the flow problem. To describe the considered hybrid nanofluid known as TiO_2-CuO/H_2O, a two-step process is employed. Firstly, titania (TiO_2) nanoparticles are uniformly dispersed into a base fluid. Subsequently, copper oxide (CuO) nanoparticles are introduced into the TiO_2/water nanofluid. Table 1 presents the thermophysical characteristics of both the base fluid and nanoparticles at a specific temperature of 25°C. Further, it is also supposed that the velocity of the free stream is $U(x) = U_\infty x^m$ and T_∞ is temperature of the ambient hybrid nanofluid, while $u_w(x) = U_w x^m$ represents velocity of a moving wedge, where U_∞, U_w, and m (within the range of 0-1) ([51, 52]) are constants and T_w is surface temperature of the wedge. Wedge angle is $\pi\beta$ such that $\beta = 2m/(m+1)$.

The governing equations of conservation of mass, momentum, and energy for hybrid nanofluid are presented as follows, employing the boundary layer approximation [39].

$$\frac{\partial u}{\partial x} + \frac{\partial v}{\partial y} = 0, \tag{1}$$

$$u\frac{\partial u}{\partial x} + v\frac{\partial u}{\partial y} = U\frac{dU}{dx} + \frac{\mu_{hnf}}{\rho_{hnf}}\frac{\partial^2 u}{\partial y^2} - B^2(x)\frac{\sigma_{hnf}}{\rho_{hnf}}(u - U) - \frac{\mu_{hnf}}{\rho_{hnf}}\frac{(u - U)}{K_0}, \tag{2}$$

$$u\frac{\partial T}{\partial x} + v\frac{\partial T}{\partial y} = \alpha_{hnf}\frac{\partial^2 T}{\partial y^2} + \frac{Q_0(T - T_\infty)}{(\rho C_p)_{hnf}} - \frac{1}{(\rho C_p)_{hnf}}\frac{\partial q_r}{\partial y}, \tag{3}$$
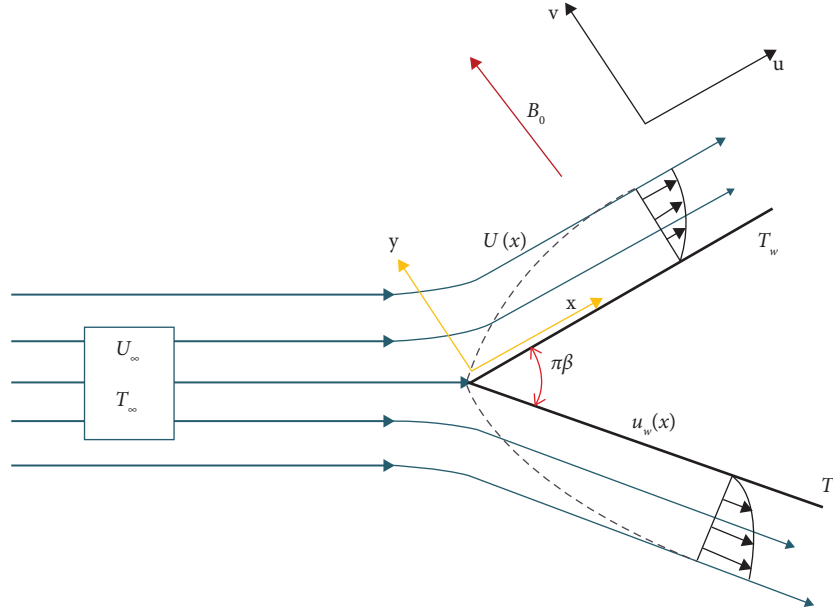
Figure 1: Visual representation and the corresponding coordinate system.

Table 1: Comprehensive thermophysical characteristics of nanoparticles and base fluid ([3, 4, 50]).

	ρ (kg/m^3)	κ (W/m K)	C_p (J/kg K)	σ (S/m)
Titania (TiO$_2$)	4250	8.9538	686.2	2.38×106
Copper oxide (CuO)	6500	17.65	533	5×10^7
Pure water	997.1	0.613	4179	0.05

and corresponding boundary conditions are as follows:

$$u = u_w(x), T = T_w, v = 0 \text{ at } y = 0; \quad (4)$$

$$u \longrightarrow U(x), T \longrightarrow T_\infty \text{ when } y \longrightarrow \infty. \quad (5)$$

Here, the varying magnetic field is $B(x) = B_0 x^{(m/2)}$ $(L/x)^{1/2}$, where B_0 is constant and L is characteristic length, $K_0 = K_1 x^{-m}(x/L)$ is the porous medium's permeability, and $Q_0 = Q_1 x^m (L/x)$ is heat generation/absorption.

Thermophysical characteristics of hybrid nanofluid in terms of their effectiveness as density ρ_{hnf}, specific heat for certain pressure $(C_p)_{hnf}$, heat capacitance $(\rho C_p)_{hnf}$, dynamic viscosity μ_{hnf}, and thermal diffusivity α_{hnf} are defined as follows ([9, 27]):

$$\rho_{hnf} = \phi(\rho_s) + (1-\phi)(\rho_f), (C_p)_{hnf} = \phi(C_p)_s + (1-\phi),$$

$$\mu_{hnf} = \frac{\mu_f}{(1-\phi)^{2.5}}, \alpha_{hnf} = \frac{\kappa_{hnf}}{(\rho C_p)_{hnf}},$$

$$(\rho C_p)_{hnf} = \left[\phi(\rho_s) + (1-\phi)(\rho_f)\right] \times \left[\phi(C_p)_s + (1-\phi)(C_p)_f\right]. \quad (6)$$

The ϕ, ρ_s, and $(C_p)_s$ provide corresponding volume fraction, density, and specific heat for certain pressure of nanoparticles. These quantities can be calculated by the following formulas (Sunder et al. [8]):

$$\rho_s = \frac{(\rho_1 \times w_1) + (\rho_2 \times w_2)}{w_1 + w_2},$$

$$(C_p)_s = \frac{\{w_1 \times (C_p)_1\} + \{w_2 \times (C_p)_2\}}{w_1 + w_2},$$

$$\phi = \frac{(w_1 + w_2/\rho_s)}{(w_f/\rho_f) + (w_1 + w_2/\rho_s)}, \quad (7)$$

$$\phi_1 = \frac{(w_1/\rho_1)}{(w_f/\rho_f) + (w_1/\rho_1) + (w_2/\rho_2)},$$

$$\phi_2 = \frac{(w_2/\rho_2)}{(w_f/\rho_f) + (w_1/\rho_1) + (w_2/\rho_2)}.$$

Here, we have three distinct masses represented by w_f, w_1, and w_2, corresponding to fundamental fluid, the initial nanoparticle, and the subsequent nanoparticle, respectively. Each nanoparticle and the base fluid are characterized by their respective densities, denoted as ρ_1, ρ_2, and ρ_f. Furthermore, the specific heats of the first and second nanoparticles are represented as $(C_p)_1$ and $(C_p)_2$, respectively. Additionally, both ϕ_1 and ϕ_2 represent the volume fraction of the initial and subsequent nanoparticles, respectively.

From the Hamilton–Crosser model ([9, 27, 46]), we enumerate thermal conductivity κ_{nf} and electric conductivity σ_{nf} of nanofluid with single particle as follows:

$$\kappa_{nf} = \frac{\kappa_1 + \kappa_f(n_1 - 1) - (\kappa_f - \kappa_1)\phi_1(n_1 - 1)}{\kappa_1 + \kappa_f(n_1 - 1) + (\kappa_f - \kappa_1)\phi_1}\kappa_f,$$

$$\sigma_{nf} = \frac{\sigma_1\{1 + (n_1 - 1)\phi_1\} + (n_1 - 1)\sigma_f(1 - \phi_1)}{\sigma_1(1 - \phi_1) + \sigma_f\{(n_1 - 1) + \phi_1\}}\sigma_f. \tag{8}$$

where n_1 is the shape factor for the nanoparticle.

Using the above model, we define thermal conductivity κ_{hnf} and electric conductivity σ_{hnf} for the hybrid nanofluid (TiO$_2$-CuO/water) as follows ([14, 46]):

$$\frac{\kappa_{hnf}}{\kappa_f} = \frac{\kappa_2 + \kappa_{nf}(n_2 - 1) - (\kappa_{nf} - \kappa_2)\phi_2(n_2 - 1)}{\kappa_2 + \kappa_{nf}(n_2 - 1) + (\kappa_{nf} - \kappa_2)\phi_2} \times \frac{\kappa_1 + \kappa_f(n_1 - 1) - (\kappa_f - \kappa_1)\phi_1(n_1 - 1)}{\kappa_1 + \kappa_f(n_1 - 1) + (\kappa_f - \kappa_1)\phi_1},$$

$$\frac{\sigma_{hnf}}{\sigma_f} = \frac{\sigma_2\{1 + \phi_2(n_2 - 1)\} + (n_2 - 1)\sigma_{nf}(1 - \phi_2)}{\sigma_2(1 - \phi_2) + \sigma_{nf}\{(n_2 - 1) + \phi_2\}} \times \frac{\sigma_1\{1 + \phi_1(n_1 - 1)\} + (n_1 - 1)\sigma_f(1 - \phi_1)}{\sigma_1(1 - \phi_1) + \sigma_f\{(n_1 - 1) + \phi_1\}}. \tag{9}$$

To determine the effect of nanoparticles on hybrid nanofluid flow, their thermophysical properties are incorporated in Table 1.

Radiative heat flux, determined through the application of the Rosseland approximation, is represented as follows:

$$q_r = -\frac{\partial T^4}{\partial y}\left(\frac{4\sigma^*}{3k^*}\right), \tag{10}$$

where k^* represents absorption coefficient, and σ^* stands for Stefan–Boltzmann constant. By disregarding higher-order terms and assuming that T^4 can be elaborated as a Taylor series about T_∞, we obtain the following equation:

$$T^4 \approx 4TT_\infty^3 - 3T_\infty^4. \tag{11}$$

Applying equation (11) to equation (10), we obtain

$$q_r = -\frac{\partial T}{\partial y}\left(\frac{16\sigma^* T_\infty^3}{3k^*}\right) \text{ and hence } \frac{\partial q_r}{\partial y} = -\frac{\partial^2 T}{\partial y^2}\left(\frac{16\sigma^* T_\infty^3}{3k^*}\right). \tag{12}$$

We utilize the subsequent similarity conversion to change the governing equations into a set of dimensionless nonlinear ODEs (White [56]):

$$\eta = \left[\frac{(m + 1)U(x)}{2v_f x}\right]^{1/2}y, \psi = \left[\frac{2v_f xU(x)}{m + 1}\right]^{1/2}f(\eta) \text{ and } \theta(\eta) = \frac{T - T_\infty}{T_w - T_\infty}. \tag{13}$$

The dimensional stream function, denoted as ψ, can be represented by the following expression:

$u = (\partial\psi/\partial y)$ and $v = -(\partial\psi/\partial x)$ are its standard form. The symbol f stands for nondimensional stream function, θ for the nondimensional temperature distribution, and η for the similarity variable.

Equations (2) and (3) are combined with equations (5), (8), (11), and (13) to create the system of nonlinear ODEs as shown in the following equation:

$$A_1 f''' + f'' f + \beta\left(1 - f'^2\right) - (2A_4 A_5 M + 2A_1 K)(f' - 1) = 0, \tag{14}$$

$$\frac{A_2}{\text{Pr}}(A_3 + R)\theta'' + f\theta' + 2A_2 Q\theta \tag{15}$$

with the coupling of boundary conditions in terms of f and θ:

$$f(\eta) = 0, \theta(\eta) = 1, f'(\eta) = \lambda \text{ at } \eta = 0; \qquad (16)$$

$$f'(\eta) \longrightarrow 1, \theta(\eta) \longrightarrow 0 \text{ when } \eta \longrightarrow \infty, \qquad (17)$$

where prime is employed to indicate the derivative concerning the variable η.

The following equations are the parameters utilized in equations (14)–(17):

$$\beta = \frac{2m}{m+1}, A_1 = \frac{\mu_{hnf}/\mu_f}{\mu_{hnf}/\mu_f}, A_2 = \frac{\left(\rho C_P\right)_f}{\left(\rho C_P\right)_{hnf}}, A_3 = \frac{\kappa_{hnf}}{\kappa_f}, A_4 = \frac{\sigma_{hnf}}{\sigma_f}, A_5 = \frac{\rho_f}{\rho_{hnf}}, \lambda = \frac{U_w}{U_\infty}, \qquad (18)$$

$$\Pr = \frac{\nu_f}{\alpha_f}, M = \frac{\sigma_f B_0^2 L}{(m+1)U_\infty \rho_f}, K = \frac{\nu_f L}{(m+1)U_\infty K_1}, Q = \frac{L Q_1}{(m+1)U_\infty \left(\rho C_P\right)_f}, R = \frac{16 T_\infty^3 \sigma^*}{3 k^* \kappa_f}. \qquad (19)$$

Here, M represents the magnetic field parameter, λ stands for parameter associated with moving wedge, K denotes the permeability parameter, Q represents the parameter related to heat absorption/generation, and R corresponds to the radiation parameter. Furthermore, we have five distinct constants: A_1, A_2, A_3, A_4, and A_5.

We encounter two significant nondimensional quantities of paramount importance; the first is the skin friction coefficient and the second is the local Nusselt number. These quantities can be precisely described in a subsequent manner:

$$C_{f_x} = \frac{\mu_{hnf}}{U^2(x)\rho_f}\left(\frac{\partial u}{\partial y}\right)_{y=0}, Nu_x = -\frac{x}{\kappa_f(T_w - T_\infty)}\left(\kappa_{hnf} + \frac{16\sigma^* T_\infty^3}{3k^*}\right)\left(\frac{\partial T}{\partial y}\right)_{y=0}, \qquad (20)$$

The reduced skin friction coefficient and the Nusselt number are determined by substituting equations (6) and (13) into equation (20) as follows:

$$\left(\frac{2Re_x}{m+1}\right)^{1/2} C_{f_x} = \frac{1}{(1-\phi)^{2.5}} f''(0), \left(\frac{2}{Re_x(m+1)}\right)^{1/2} Nu_x = -\left(\frac{\kappa_{hnf}}{\kappa_f} + R\right)\theta'(0), \qquad (21)$$

where $Re_x = (U(x)x/\nu_f)$ represents the local Reynolds number.

2. Numerical Method

By using the in-built function "bvp4c" in MATLAB software, the nondimensional momentum equation (14) and energy equation (15) have been numerically solved along with the associated boundary conditions (15). The bvp4c method in MATLAB offers several advantages compared to other methods for solving boundary value problems (BVPs). One notable strength lies in its versatility, as bvp4c is well-suited for handling a wide range of linear and nonlinear BVPs arising from various scientific and engineering applications. It employs a collocation approach, which discretizes the problem domain into a set of collocation points, providing accurate and stable solutions. The adaptive mesh refinement feature enhances efficiency by automatically adjusting the grid during the solution process, optimizing computational

resources. Additionally, bvp4c supports a user-friendly interface, simplifying the implementation of complex BVPs. Its robustness, flexibility, and efficiency make bvp4c a preferred choice for researchers and engineers when tackling diverse boundary value problems within the MATLAB environment. In order to convert resulting boundary layer equations into ODEs of first-order in the present problem, the following terms are introduced to the following equation:

$$\begin{aligned} f &= f_1, \\ f' &= f_2, \\ f'' &= f_3, \\ \theta &= f_4, \\ \theta' &= f_5. \end{aligned} \qquad (22)$$

Using the abovementioned substitutions, the following system of first-order ODEs is obtained:

$$f_1' = f_2,$$

$$f_2' = f_3,$$

$$f_3' = \left(\frac{1}{A_1}\right)\left[(f_2^2 - 1)\beta - f_1 f_3 + (2A_4 A_5 M + 2A_1 K)(f_2 - 1)\right],$$

$$f_4' = f_5,$$

$$f_5' = -\left\{\frac{Pr}{A_2(A_3 + R)}\{\}[f_1 f_5 + 2A_2 Q f_4]\right\}.$$

$$(23)$$

with initial conditions

$$\eta = 0: f_1 = 0, f_2 = \lambda, f_3 = \alpha_{10}, f_4 = 1, f_5 = \alpha_{20}. \quad (24)$$

Here, α_{10} and α_{20} are unknown quantities. The first time we assume these unknowns and afterward, these are approximated within bvp4c coding itself such that boundary conditions at $\eta \longrightarrow \infty$, i.e., $f_2 \longrightarrow 1$ and $f_4 \longrightarrow 0$ are satisfied. From the computational point of view, we have considered η in the interval $[0, 5]$ instead of the unbounded interval $[0, \infty)$. We employed a step size $h = 0.05$ and an error tolerance value 1×10^{-3} for computational accuracy. For the validation of our "bvp4c" code, we have also prepared a MATLAB code of Runge–Kutta fourth-order method along with shooting technique (RK-S) for the present problem taking the same step size and error tolerance, and results are presented in tabular form.

3. Results and Discussion

Using the in-built function "bvp4c" in the MATLAB software, we perform numerical analysis of the system of dimensionless ODEs represented by equation (23) with associated boundary conditions specified in equation (24). The parameters we consider for the computation fall within a specific range of values such as $1.0 \le K \le 3.0$, $1.0 \le M \le 3.0$, $-5.0 \le Q \le 5.0$, $0.1 \le R \le 2.0$, $-0.6 \le \lambda \le 0.6$, $3.0 \le n_1 \le 5.7$, $3.0 \le n_2 \le 5.7$, $0.0 \le \phi \le 0.1002$, $0.0 \le \phi_1 \le 0.630$, $0.0 \le \phi_2 \le 0.412$, and $0 \le \beta \le 1$. The standard values of parameters are taken into account during the entire process of numerical computations as $K = 1.0$, $M = 1.0$, $Pr = 6.2$, $Q = 0.1$, $R = 0.1$, $\beta = 1/3$ ($m = 0.2$) and $\lambda = -0.4$ unless stated separately. In the present study, we have used nanoparticles with four distinct kinds of shape which are sphere, brick, cylinder, and platelets; further corresponding values of shape factor parameter (n) for these shapes are 3.0, 3.7, 4.9, and 5.7, respectively. In the present study, $\lambda > 0$ indicates that both wedge and fluid are moving in same direction, whereas $\lambda < 0$ signifies that wedge and fluid are moving in opposite directions.

Initially, the impact of varying inputs of permeability parameter (K) on velocity and temperature profiles is illustrated in Figures 2 and 3, correspondingly. With an enhancement in permeability parameter (K), the nature of velocity and temperature profiles exhibit distinct characteristics. Figure 2(a) shows that when $\lambda < 0$ ($\lambda = -0.4$), velocity profiles improve with an increment in data of K. When $\lambda > 0$, velocity profiles increase for $\lambda = 0.4$ while these profiles drop down for $\lambda = 1.4$ with the rise in inputs of K, as seen in diagram 2(b). Figure 3(a) declares that when $\lambda < 0$ ($\lambda = -0.4$), the temperature profiles fall as the values of permeability parameter (K) grow. Figure 3(b) shows that when $\lambda > 0$, the temperature profiles reduce for $\lambda = 0.4$ and increases for $\lambda = 1.4$ as values of K increase. Figures 4 and 5 illustrate how changes in magnetic field parameter (M) influence both velocity and temperature distributions. Figure 4(a) reveals that when M increases, the velocity profiles for the present hybrid nanofluid accelerate when $\lambda < 0$ ($\lambda = -0.4$). As demonstrated by Figure 4(b), when $\lambda > 0$, the velocity profiles increase for $\lambda = 0.4$ while they diminish for $\lambda = 1.4$ as the value of M increases. When charged particles, such as electrons or ions, move through a magnetic field, they experience a force known as the Lorentz force. The magnitude and direction of this force depend on the charge of the particle, its velocity, and the strength and orientation of the magnetic field. If the direction of the magnetic field remains constant, an increase in the magnetic field strength will result in a stronger force acting on the charged particle; therefore, the velocity of the fluid reduces for increasing values of the magnetic field parameter. The particle might experience acceleration or deceleration, depending on its initial velocity. In the current investigation, when the free stream velocity surpasses the wedge velocity, an escalation in the magnetic field parameter results in an increase in fluid velocity. Conversely, when the wedge velocity exceeds the free stream velocity, the fluid velocity experiences a decrease for escalating values of the magnetic field parameter. According to Figure 5(a), when $\lambda < 0$ ($\lambda = -0.4$), temperature profiles decline as value of magnetic parameter (M) grows. As seen in Figure 5(b), when $\lambda > 0$, the temperature profiles reduce for $\lambda < 1$ and increase for $\lambda > 1$ as the value of M increases. Figure 6 illustrates how changes in heat absorption/generation parameter (Q) influence the temperature profile. It confirms that improved inputs of Q cause an elevation in temperature profiles. On the other hand, Figure 7 shows how the temperature profile is affected by the radiation absorption parameter (R). The observation drawn from this graph indicates that an improvement in R creates
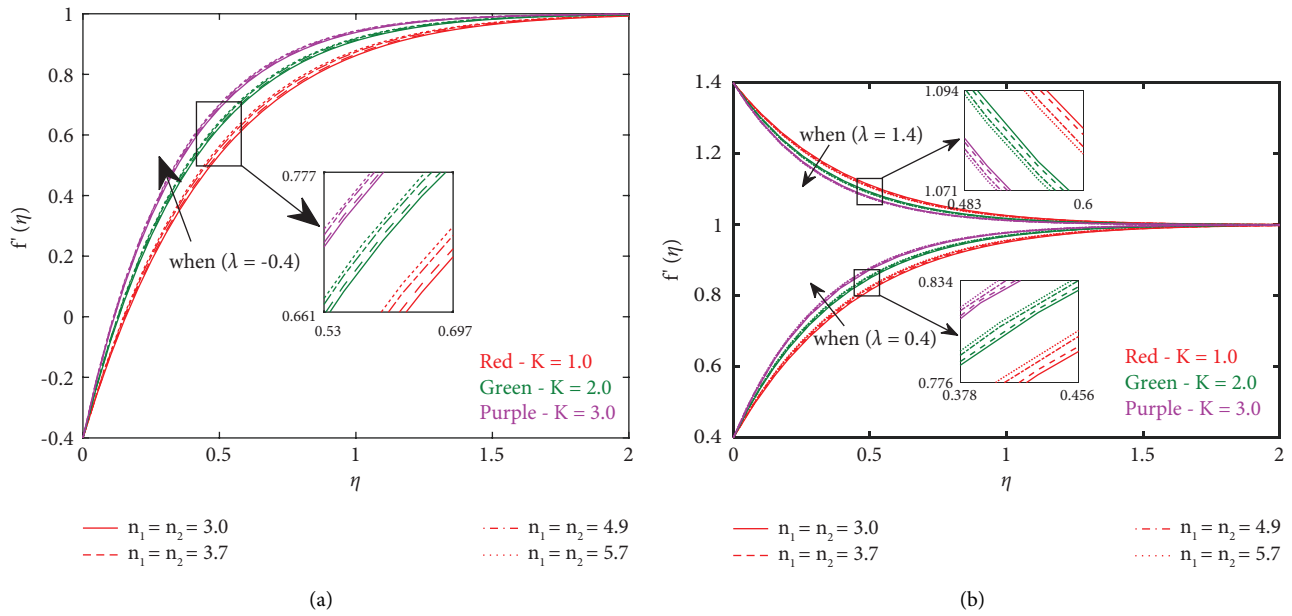
FIGURE 2: Influence of K along with n_1 and n_2 on velocity profile when (a) $\lambda < 0$ and (b) $\lambda > 0$.
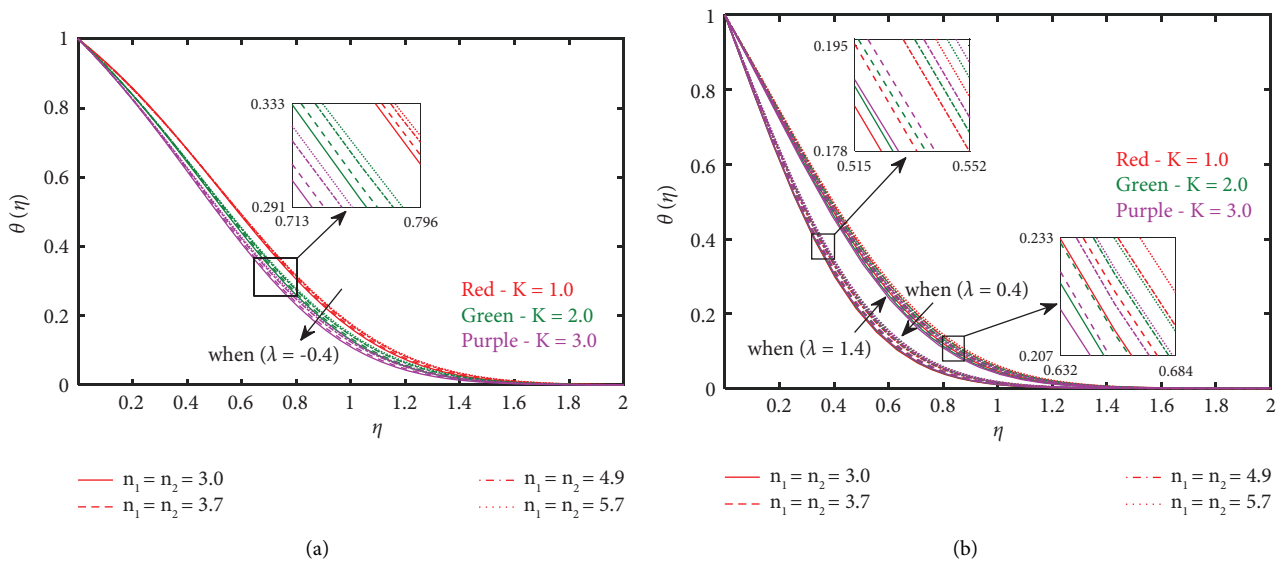

FIGURE 3: Influence of K along with n_1 and n_2 on temperature profile when (a) $\lambda < 0$ and (b) $\lambda > 0$.

a corresponding enhancement in the temperature profiles of the nanofluid. As the radiation absorption parameter rises, there is an associated increase in the internal energy of the nanofluid, resulting in a temperature elevation. This temperature rise is attributed to the conversion of absorbed energy into heat, consequently raising the internal energy of the nanofluid. Figure 8 has been constructed to examine the effect of the dynamic wedge parameter (λ) on velocity distribution, and observation from this diagram illustrates that the velocity profile for the hybrid nanofluid is higher when $\lambda > 0$, while the velocity profile of the hybrid nanofluid is lesser when $\lambda < 0$. Figure 9 illustrates how the temperature

profile is affected by variations in the moving wedge parameter (λ). It is indicated that for raising inputs of λ, temperature profiles decrease. In addition to Figure 6, it is concluded by Figures 2–9 that growing values of the shape factor parameter $(n_2$ and $n_2)$ enhance the velocity and temperature profiles for the nanofluid flow across a moving/ static wedge, together with magnetic field effects, thermal radiation effects, and the porous medium parameter. Figure 6 illustrates that the shape factor exerts a greater influence on temperature distribution, particularly when the heat generation parameter (Q) attains higher values. Simultaneously, the effect of shape factors $(n_1$ and $n_1)$ becomes
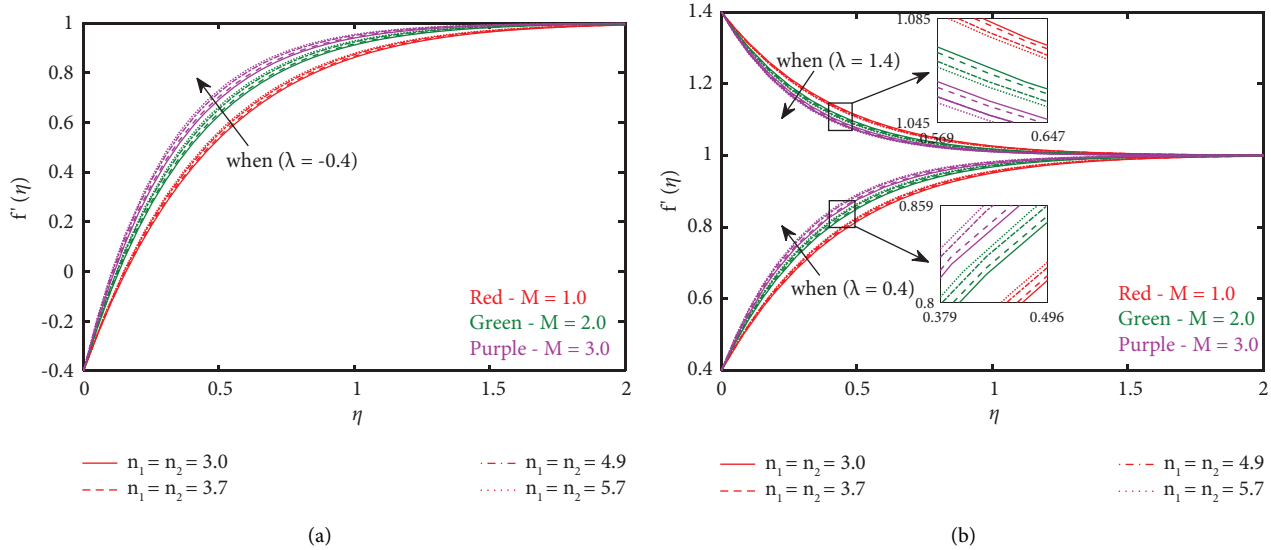
FIGURE 4: Influence of M along with n_1 and n_2 on velocity profile when (a) $\lambda < 0$ and (b) $\lambda > 0$.
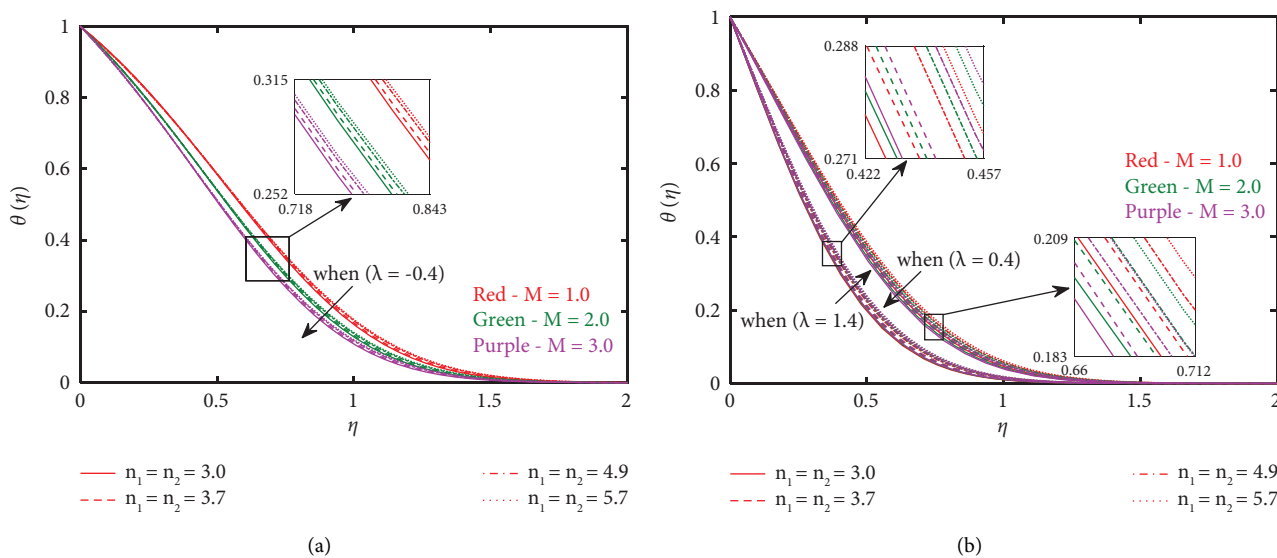

FIGURE 5: Influence of M along with n_1 and n_2 on temperature profile when (a) $\lambda < 0$ and (b) $\lambda > 0$.

negligible for increasing values of R, which is clearly observed in Figure 7. Here, static wedge is represented by $\lambda = 0$. The Hartree pressure gradient parameter, denoted by β, signifies a complete wedge angle, represented by $\beta\pi$. Further, $\beta = 1(m = 1)$ demonstrates boundary layer flow in the vicinity of the stagnation point of an upright flat plate, $\beta = 1/3$ ($m = 0.2$) represents the wedge flow with a complete angle $\pi/3$, and $\beta = 0$ ($m = 0$) reflects the flow over a smooth horizontal plate. An opposite pattern is observed in Figure 10 for both velocity and temperature patterns with distinct values of β. Figure 10 displays that velocity profiles of hybrid nanofluid continuously diminish while temperature profiles of the same increase when boundary layer flow shifts their position from the stagnation point of an upright smooth plate to a horizontal flat plate. Figures 11 and 12 show, respectively, a comparison of $[(2Re_x)/(m + 1)]^{1/2}C_{f_x}$ (local

skin friction coefficient) and $[2/\{Re_x (m + 1)\}]^{1/2}Nu_x$ (local Nusselt number) in terms of various values of w_1 and w_2 by considering $\lambda = -0.4$ and $\lambda = 0.3$. Figures 11 and 12 exhibit that whenever mass of each nanoparticle enhances, so does $[(2Re_x)/(m + 1)]^{1/2}C_{f_x}$ and $[2/\{Re_x (m + 1)\}]^{1/2}Nu_x$. Furthermore, the skin friction coefficient for $\lambda = 0.3$ is less than that of $\lambda = -0.4$, and the local Nusselt number for $\lambda = 0.3$ is larger than that of $\lambda = -0.4$. Based on these findings, it is possible to conclude that flow of hybrid nanofluid over a wedge considering that both fluid and wedge are moving in the same direction ($\lambda > 0$) gives better results when compared with the opposite direction movement ($\lambda < 0$). Of all the fluid models we are considering here, the highest $[2/\{Re_x (m + 1)\}]^{1/2}Nu_x$ (heat transfer rate) and greatest $[(2Re_x)/(m + 1)]^{1/2}C_{f_x}$ (skin friction coefficient) occurs in case of HNF4 hybrid nanofluid model for both $\lambda = -0.4$ and
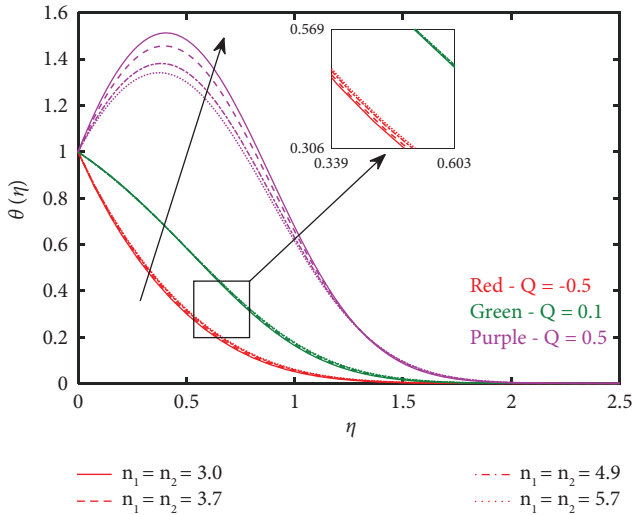
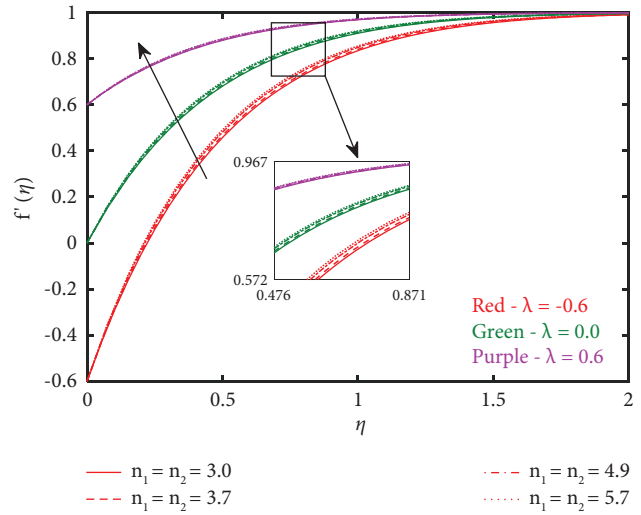FIGURE 6: Influence of Q and shape factor n_1 and n_2 on temperature profile.

FIGURE 8: Influence of λ and shape factor n_1 and n_2 on velocity profile.
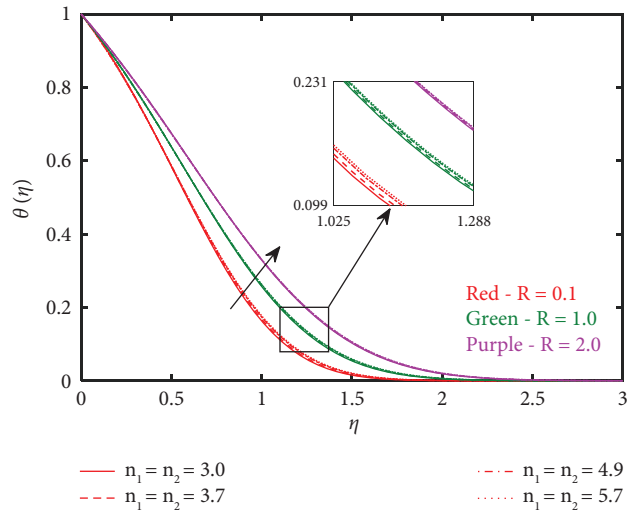

FIGURE 7: Influence of R and shape factor n_1 and n_2 on temperature profile.
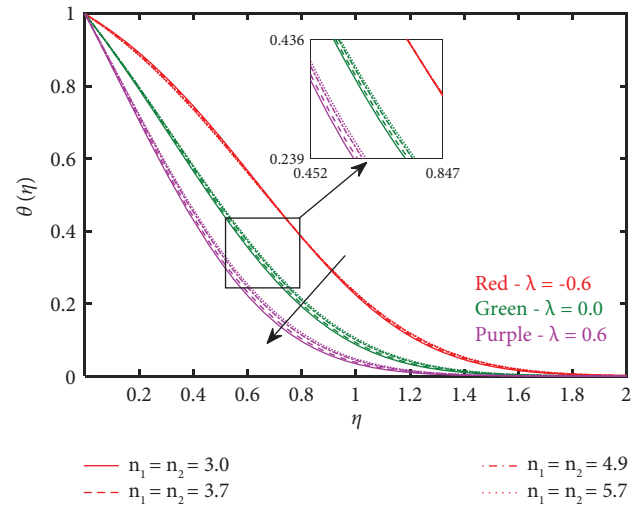

FIGURE 9: Influence of λ and shape factor n_1 and n_2 on temperature profile.

$\lambda = 0.3$, which highlight the benefits of using hybrid nanofluid over single nanofluid and pure water. Of all the nanoparticle's shape we are considering here, the highest $[2/\{Re_x(m+1)\}]^{1/2}Nu_x$ (heat transfer rate) occurs in case of platelet shape ($n_1 = n_2 = 5.7$) of nanoparticles for both $\lambda = -0.4$ and $\lambda = 1.4$. Table 2 conveys the standard values of the shape factor parameter (n) of nanoparticles, and Table 3 indicates the various kinds of fluid situations investigated for the present study. Admirable results ([38, 39, 44]) have been detected on viewing Table 4, which is formulated for the $[(2Re_x)/(m+1)]^{1/2}C_{f_x}$ (local skin friction coefficient) considering fluid as pure water ($\phi = \phi_1 = \phi_2 = 0$), static wedge ($\lambda = 0$), and several values of β. Table 5, which is formulated for $[(2Re_x)/(m+1)]^{1/2}C_{f_x}$, and Table 6, which is formed for $2/\{Re_x(m+1)\}]^{1/2}Nu_x$ (using Maxwell–Garnet model for κ_{hnf}/κ_f [39]) considering TiO$_2$-water nanofluid

(i.e., $\phi_2 = 0$) and static wedge (i.e., $\lambda = 0$) with various values of $\phi = \phi_1$ and β, also gives good agreement with published results ([39, 44]).

Table 7 displays variations in $[(2Re_x)/(m+1)]^{1/2}C_{f_x}$ for a variety of numerical inputs assigned to parameters employed in the present investigation using the bvp4c and the RK fourth-order method with shooting technique (RK-S). Table 8 presents a summary of alterations in $[2/\{Re_x(m+1)\}]^{1/2}Nu_x$ across various numerical inputs assigned to the parameters analyzed in this study. These calculations were performed using the bvp4c method and the RK 4th order method with a shooting technique (RK-S). Additionally, Table 7, it is observed that larger inputs of K, M, and β correspond to an increase in the $[(2Re_x)/(m+1)]^{1/2}C_{f_x}$, while contrary outcomes observed for λ. Examining the data in Table 8 allows us to conclude
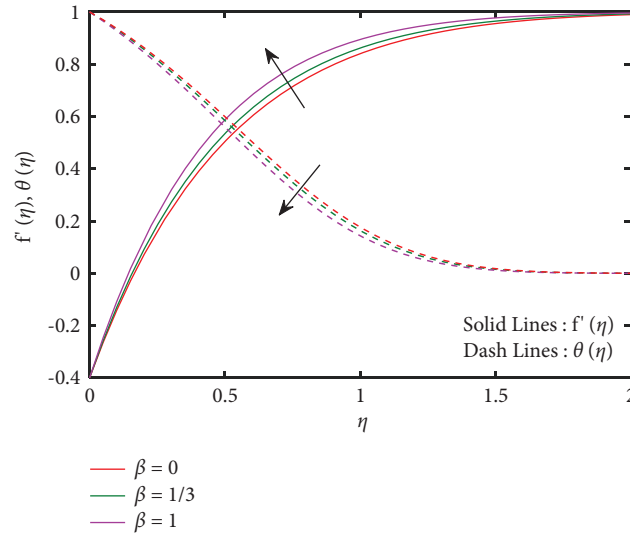
FIGURE 10: Influence of β on velocity and temperature profiles when $n_1 = n_2 = 3$.

	RF	NF1	NF2	NF3	NF4	HNF1	HNF2	HNF3	HNF4
■ $\lambda = 0.3$	1.5319	1.6778	1.8278	1.6333	1.7361	1.7751	1.8791	1.9247	2.0293
■ $\lambda = -0.4$	2.9336	3.2114	3.4983	3.1208	3.3116	3.3913	3.5851	3.6781	3.8736
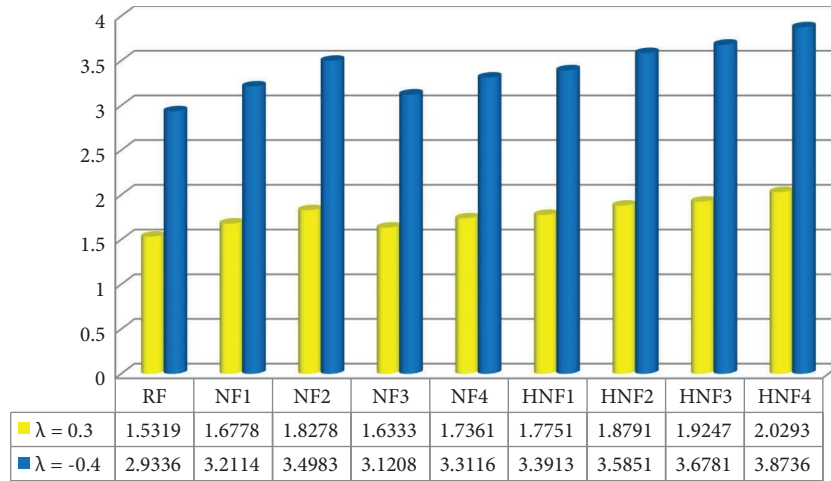
FIGURE 11: Local skin friction coefficient $[(2Re_x)/(m+1)]^{1/2} C_{f_x}$ of TiO$_2$-CuO/water hybrid nanofluid estimated for several values of w_1 and w_2, when $w_f = 100$ gm and $n_1 = n_2 = 3$.

	RF	NF1	NF2	NF3	NF4	HNF1	HNF2	HNF3	HNF4
■ $\lambda = 0.3$	1.2068	1.3355	1.4531	1.3394	1.4619	1.4632	1.5791	1.5749	1.6855
■ $\lambda = -0.4$	0.5398	0.6294	0.7112	0.6274	0.7077	0.7142	0.7905	0.7925	0.8658

FIGURE 12: Local Nusselt number $[2/\{Re_x(m+1)\}]^{1/2} Nu_x$ of TiO$_2$-CuO/water hybrid nanofluid estimated for several values of w_1 and w_2, when $w_f = 100$ gm and $n_1 = n_2 = 3$.

TABLE 2: Different fluid models considered for the study.

Type	RF	NF1	NF2	NF3	NF4	HNF1	HNF2	HNF3	HNF4
w_f (gm)	100	100	100	100	100	100	100	100	100
w_1 (gm)	0	15	30	0	0	15	15	30	30
w_2 (gm)	0	0	0	15	30	15	30	15	30

TABLE 3: The prevalent values for nanoparticle shape factor (n).

S. no.	1	2	3	4
Shapes of nanoparticles	Spherical	Brick	Cylinder	Platelet
Structure				
n	3.0	3.7	4.9	5.7

TABLE 4: Comparison of numerous values of $f''(0)$ (skin friction coefficient) for various values of β, when $M = K = \lambda = \phi = \phi_1 = \phi_2 = w_1 = w_2 = 0$ and $w_f = 100$ gm.
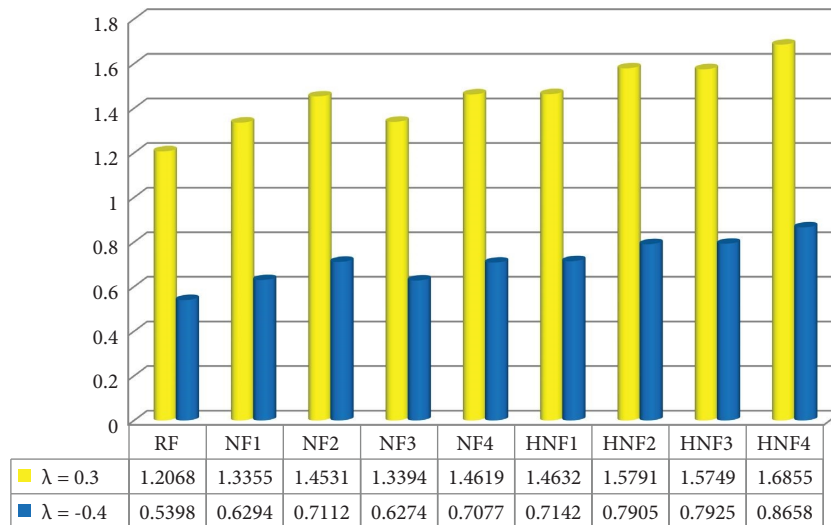
β	Dinarvand et al. [44]	Ishak et al. [38]	Yacob et al. [39]	Present study bvp4c	Present study RK-S
0	0.469600	0.4696	0.4696	0.469645	0.469645
1/6	0.654993	0.6550	0.6550	0.655000	0.655000
1/3	0.802125	0.8021	0.8021	0.802127	0.802127
1/2	0.927680	0.9277	0.9277	0.927680	0.927680
4/7	0.976824	—	—	0.976825	0.976825
10/15	1.038900	—	1.0389	1.038903	1.038903
1	1.232587	1.2326	1.2326	1.232587	1.232587

TABLE 5: Comparison of the values of skin friction coefficient $[(2Re_x)/(m+1)]^{(/)}C_{f_x}$ for several values of β and $\phi = \phi_1$ (TiO$_2$-water nanofluid), $\phi_2 = 0$, when $M = K = \lambda = 0$ and $n_1 = 3$.

β	$\phi = \phi_1$	$[(2Re_x)/(m+1)]^{(/)}C_{fx}$ Dinarvad et al. [44]	Yacob et al. [39]	Present study bvp4c	Present study RK-S
0	0.1	0.616929	0.6169	0.616978	0.616978
	0.2	0.797872	0.7978	0.798002	0.798002
10/15 ($m = 0.5$)	0.1	1.364842	1.3648	1.364842	1.364842
	0.2	1.765142	1.7651	1.765143	1.765143
1	0.1	1.619291	1.6192	1.619291	1.619291
	0.2	2.094220	2.0942	2.094220	2.094220

TABLE 6: Comparison of the values of local Nusselt number $[2/\{Re_x(m+1)\}]^{1/2}Nu_x$ for several values of β and $\phi = \phi_1$ (TiO$_2$-water nanofluid), $\phi_2 = 0$, when $M = Q = R = K = \lambda = 0$, $n_1 = 3$, and Pr $= 6.2$.

β	$\phi = \phi_1$	$[2/\{Re_x(m+1)\}]^{1/2}Nu_x$ Dinarvad et al. [44]	Yacob et al. [39]	Present study bvp4c	Present study RK-S
0	0.1	1.018845	1.0189	1.018872	1.018872
	0.2	1.156053	1.1561	1.156116	1.156116
10/15 ($m = 0.5$)	0.1	1.246064	1.2460	1.246064	1.246064
	0.2	1.408206	1.4082	1.408205	1.408205
1	0.1	1.301085	1.3010	1.301084	1.301084
	0.2	1.469032	1.4691	1.469032	1.469032

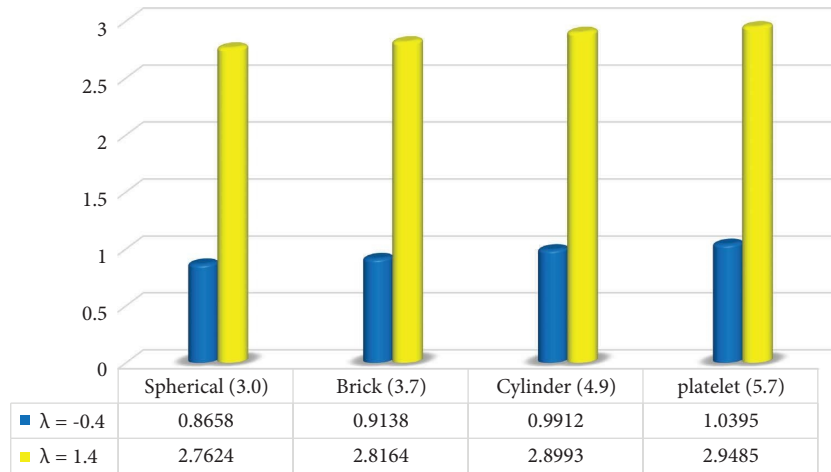|	Spherical (3.0)	Brick (3.7)	Cylinder (4.9)	platelet (5.7)
■ $\lambda = -0.4$	0.8658	0.9138	0.9912	1.0395
■ $\lambda = 1.4$	2.7624	2.8164	2.8993	2.9485

FIGURE 13: Local Nusselt number $[2/\{Re_x\,(m+1)\}]^{1/2}Nu_x$ for different shape factor values ($n_1 = n_2$), when $w_1 = w_2 = 30\,$gm, $w_f = 100\,$gm, $K = 1.0$, $M = 1.0$, $\mathrm{Pr} = 6.2$, $Q = 0.1$, $R = 0.1$, and $\beta = 1/3$ ($m = 0.2$).

TABLE 7: Numerical values of skin friction coefficient $[(2Re_x)/(m+1)]^{1/2}C_{f_x}$, when $w_1 = w_2 = 30\,$gm, $w_f = 100\,$gm, $n_1 = n_2 = 3$, $Q = 0.1$, and $R = 0.1$.

K	M	β	λ	$[(2Re_x)/(m+1)]^{1/2}C_{fx}$	
				bvp4c	RK-S
1.0	1.0	1/3	−0.4	3.873648	3.873648
2.0				4.652700	4.652700
3.0				5.318913	5.318913
1.0	2.0	1/3	−0.4	4.682742	4.682742
	3.0			5.371386	5.371386
1.0	1.0	0	−0.4	3.701487	3.701486
		1		4.196968	4.196966
1.0	1.0	1/3	0.3	2.029297	2.029297
			1.4	−1.238629	−1.238629

TABLE 8: Numerical values of local Nusselt number $[2/\{Re_x\,(m+1)\}]^{1/2}Nu_x$, when $\mathrm{Pr} = 6.2$, $w_1 = w_2 = 30\,$gm, $w_f = 100\,$gm, and $n_1 = n_2 = 3$.

K	M	β	R	Q	λ	$[2/\{Re_x\,(m+1)\}]^{1/2}Nu_x$	
						bvp4c	RK-S
1.0	1.0	1/3	0.1	0.1	−0.4	0.865840	0.865839
2.0						1.006022	1.006022
3.0						1.104281	1.104281
1.0	2.0	1/3	0.1	0.1	−0.4	1.010828	1.010828
	3.0					1.111351	1.111350
1.0	1.0	0	0.1	0.1	−0.4	0.820067	0.820066
		1				0.943022	0.943024
1.0	1.0	1/3	1.0	0.1	−0.4	1.365100	1.365100
			2.0			1.842555	1.842554
1.0	1.0	1/3	0.1	−0.5	−0.4	3.002588	3.002585
				0.5		−3.287662	−3.287664
1.0	1.0	1/3	0.1	0.1	0.3	1.685550	1.685550
					1.4	2.762437	2.762434

a definite conclusion regarding the hybrid nanofluid model HNF4; the $[2/\{Re_x\,(m+1)\}]^{1/2}Nu_x$ shows a tendency to decrease as inputs of parameter Q improve. Conversely, the parameters K, M, R, λ, and β demonstrate an opposing trend, where their increasing values lead to an escalation in the $[2/\{Re_x\,(m+1)\}]^{1/2}Nu_x$. To validate the results obtained

from our present method "bvp4c," we also perform calculations using Runge–Kutta fourth-order method along with shooting technique. From Tables 4 to 8, we also observe that the results obtained via both methods i.e., bvp4c and RK-S have good agreement upto 6 decimal places which emphasize on validity of our used bvp4c code. Using both

TABLE 9: Numerical values of residual errors at the boundary ($\eta = 5$) when $Pr = 6.2$, $w_1 = w_2 = 30$ gm, $w_f = 100$ gm, and $n_1 = n_2 = 3$.

K	M	β	R	Q	λ	Residual error for velocity profiles		Residual error for temperature profiles	
						bvp4c	RK-S	bvp4c	RK-S
1.0	1.0	1/3	0.1	0.1	−0.4	2.489×10^{-4}	1.949×10^{-5}	-1.877×10^{-9}	-5.202×10^{-7}
2.0						6.911×10^{-5}	5.042×10^{-5}	3.908×10^{-12}	-2.831×10^{-7}
3.0						2.732×10^{-5}	4.572×10^{-5}	-7.317×10^{-10}	-2.071×10^{-7}
1.0	2.0	1/3	0.1	0.1	−0.4	6.579×10^{-5}	6.160×10^{-5}	9.470×10^{-11}	-2.942×10^{-7}
	3.0					2.511×10^{-5}	9.132×10^{-5}	-7.359×10^{-10}	-1.833×10^{-7}
1.0	1.0	0	0.1	0.1	−0.4	1.771×10^{-4}	6.920×10^{-5}	-8.378×10^{-10}	-1.322×10^{-8}
		1				1.276×10^{-4}	8.055×10^{-5}	3.612×10^{-8}	-1.933×10^{-7}
1.0	1.0	1/3	1.0	0.1	−0.4	2.489×10^{-4}	1.949×10^{-5}	-1.529×10^{-6}	-1.023×10^{-6}
			2.0			2.489×10^{-4}	1.949×10^{-5}	-1.232×10^{-4}	-1.199×10^{-7}
1.0	1.0	1/3	0.1	−0.5	−0.4	2.489×10^{-4}	1.949×10^{-5}	-1.623×10^{-13}	-2.413×10^{-7}
				0.5		2.489×10^{-4}	1.949×10^{-5}	-3.312×10^{-4}	-1.526×10^{-9}
1.0	1.0	1/3	0.1	0.1	0.3	1.011×10^{-4}	9.173×10^{-6}	6.288×10^{-9}	-2.703×10^{-8}
					1.4	-7.360×10^{-5}	3.584×10^{-5}	-5.015×10^{-9}	-3.922×10^{-9}

methods, bvp4c and RK-S, we have also calculated residual error in the boundary conditions at $\eta = 5$ (in place of $\eta \longrightarrow \infty$) and the same are presented in Table 9.

4. Conclusions

This article delves into the analysis of a steady and incompressible movement of an electrically conducting hybrid nanofluid (TiO_2-CuO/H_2O) over a moving wedge, while taking into account some extra effects such as a porous medium, thermal radiation, and magnetic field. Here, we have applied a mass-based strategy to develop a one-step hybrid nanofluid model. The main goal of this study is to identify how the behavior of the TiO_2-CuO/H_2O hybrid nanofluid flow is influenced by varying values of shape factor and masses of nanoparticle. Similarity transformations and bvp4c coding are utilized to solve the current issue and results are obtained via MATLAB. Some major conclusions are summarized as follows:

(i) The velocity profiles improve with larger values of the shape factor parameter for $\lambda < 1$, while declines for $\lambda > 1$.

(ii) The shape factor is more effective for rich inputs of heat absorption/generation parameter (Q) in the temperature profile.

(iii) As the permeability parameter and magnetic field parameter increase, a notable rise in velocity profiles is observed when $\lambda < 1$. Moreover, when $\lambda > 1$, a decline in velocity profiles is detected.

(iv) Presence of moving wedge parameter supports heat transfer enhancement when a wedge moves in the direction of fluid motion.

(v) Addition of masses for each nanoparticle to the fundamental fluid improves the heat transfer rate as well as the shear stress.

(vi) In our considered values of λ, maximum local Nusselt number has been observed for $\lambda = 0.3$ and largest skin friction coefficient obtained for $\lambda = -0.4$ in case of HNF4 hybrid nanofluid model.

(vii) The implication of the shape factor on temperature profiles exhibits an opposing trend to that of the impact of radiation absorption parameter when considering the same profiles.

(viii) The heat transfer rate accelerates as the complete wedge angle is extended.

The incorporation of nanoparticles to improve heat transfer has the potential to make various industries, such as manufacturing, power generation, and chemical processing, more energy-efficient. In aerospace, understanding how fluids move over surfaces, like wedges, is crucial. By experimenting with different types of nanoparticles in terms of shapes and masses, new nanofluids could be created for specific purposes beyond the current study. These applications range from biomedicine to advanced electronics cooling. Exploring how nanoparticle characteristics impact fluid flow could also aid in designing optimized nanoparticles for tasks like catalysis, sensing, and delivering drugs.

In the realm of fluid dynamics and heat transfer, further research could explore the incorporation of more sophisticated nanofluid formulations and advanced hybrid models to enhance the accuracy of predictions. Additionally, the exploration of novel materials and innovative techniques for embedding wedges in porous media could expand the range of practical scenarios to which the model can be applied. Integration with emerging technologies could also contribute to refining the model's predictive capabilities. Moreover, the validation of the model through experimental studies and real-world applications could establish its reliability and foster its adoption in diverse industrial and engineering contexts, thereby contributing to the development of more efficient and sustainable thermal management systems.

Nomenclature

B_0: Magnetic field strength (Kg s^{-2}A^{-1})
C_p: Specific heat for certain pressure (J/kgK)
K_0: Permeability of the porous medium (m^2)

f: Dimensionless stream function
M: Magnetic field parameter
T: Temperature of the nanofluid (K)
Nu: Nusselt number
K: Permeability parameter
Q_0:   Heat absorption/generation coefficient (W/m^{2}K)
n: Shape factor parameter
C_f: Skin friction coefficient
m: Falkner–Skan power law parameter
Re: Reynolds number
T_∞: Ambient temperature (K)
Pr: Prandtl number
Q: Heat absorption/generation parameter
R: Radiation absorption parameter
T_w: Wall temperature (K)
u_w: Moving wedge velocity (m/s)
u, v: Velocity component along x- and y-direction (m/s)
W: Weight of nanoparticles (kg)

Greek symbols
ρ: Density (kg/m^3)
ϕ: Volume fraction of nanoparticles
θ: Dimensionless temperature
μ: Dynamic viscosity (kg/ms)
η: Similarity variable
σ: Electric conductivity (Kg^{-1}m^{-2}s^{3}A^2)
v: Kinematic viscosity (m^2/s)
β: Hartree pressure gradient parameter
α: Thermal diffusivity (m^2/s)
λ: Moving wedge parameter
κ: Thermal conductivity (m^2/s)

Subscript
1:       TiO$_2$ nanoparticles
2:       CuO nanoparticles
hnf: Hybrid nanofluid
nf: Nanofluid
F: Base fluid
2:       Mathematical formulation.

Data Availability

The data used to support the findings of this study are made available by the corresponding author upon request.

Conflicts of Interest

The authors declare that they have no conflicts of interest.

Authors' Contributions

All authors listed have made a substantial, direct, and intellectual contribution to the work and approved it for publication.

References

[1] S. U. S. Choi, *Enhancing thermal conductivity of fluids with nanoparticles*, vol. 231, ASME Publications-Fed, New York, NY. USA, 1995.

[2] B. Takabi and H. Shokouhmand, "Effects of Al_2O_3- Cu/water hybrid nanofluid on heat transfer and flow characteristics in turbulent regime," *International Journal of Modern Physics C*, vol. 26, no. 4, 2015.

[3] A. K. Nayak, R. K. Singh, and P. P. Kulkarni, "Measurement of volumetric thermal expansion coefficient of various nanofluids," *Technical Physics Letters*, vol. 36, no. 8, pp. 696–698, 2010.

[4] S. Dinarvand and I. Pop, "Free-convective flow of copper/water nanofluid about a rotating down-pointing cone using Tiwari-Das nanofluid scheme," *Advanced Powder Technology*, vol. 28, no. 3, pp. 900–909, 2017.

[5] S. Jana, A. Salehi-Khojin, and W. H. Zhong, "Enhancement of fluid thermal conductivity by the addition of single and hybrid nano-additives," *Thermochimica Acta*, vol. 462, no. 1-2, pp. 45–55, 2007.

[6] M. Baghbanzadeh, A. Rashidi, D. Rashtchian, R. Lotfi, and A. Amrollahi, "Synthesis of spherical silica/multiwall carbon nanotubes hybrid nanostructures and investigation of thermal conductivity of related nanofluids," *Thermochimica Acta*, vol. 549, pp. 87–94, 2012.

[7] M. Nuim Labib, M. J. Nine, H. Afrianto, H. Chung, and H. Jeong, "Numerical investigation on effect of base fluids and hybrid nanofluid in forced convective heat transfer," *International Journal of Thermal Sciences*, vol. 71, pp. 163–171, 2013.

[8] L. S. Sundar, K. V. Sharma, M. K. Singh, and A. C. M. Sousa, "Hybrid nanofluids preparation, thermal properties, heat transfer and friction factor – a review," *Renewable and Sustainable Energy Reviews*, vol. 68, pp. 185–198, 2017.

[9] T. Hayat and S. Nadeem, "Heat transfer enhancement with Ag-CuO/water hybrid nanofluid," *Results in Physics*, vol. 7, pp. 2317–2324, 2017.

[10] R. Garia, S. K. Rawat, M. Kumar, and M. Yaseen, "Hybrid nanofluid flow over two different geometries with Cattaneo–Christov heat flux model and heat generation: a model with correlation coefficient and probable error," *Chinese Journal of Physics*, vol. 74, pp. 421–439, 2021.

[11] K. Jat and K. Sharma, "Unsteady MHD flow of tangent hyperbolic nanofluid over an inclined stretching sheet and heat transfer analysis," *NanoWorld Journal*, vol. 8, no. S1, pp. S104–S110, 2022.

[12] G. G. Momin, "Experimental investigation of mixed convection with water-Al_2O_3 and hybrid nanofluid in inclined tube for laminar flow," *International Journal of Scientific and Technology Research*, vol. 2, pp. 195–202, 2013.

[13] S. Suresh, K. P. Venkitaraj, P. Selvakumar, and M. Chandrasekar, "Effect of Al_2O_3–Cu/water hybrid nanofluid in heat transfer," *Experimental Thermal and Fluid Science*, vol. 38, pp. 54–60, 2012.

[14] H. Xu and Q. Sun, "Generalized hybrid nanofluid model with the application of fully developed mixed convection flow in a vertical Microchannel∗," *Communications in Theoretical Physics*, vol. 71, no. 8, pp. 903–911, 2019.

[15] M. Sagheer, S. Shah, S. Hussain, and M. Akhtar, "Impact of non-uniform heat source/sink on magnetohydrodynamic Maxwell nanofluid flow over a convectively heated stretching surface with chemical reaction," *Journal of Nanofluids*, vol. 8, no. 4, pp. 795–805, 2019.

[16] S. Shah, S. Hussain, M. Sagheer, and M. Bilal, "Numerical study of three dimensional mixed convective Maxwell nanofluid flow over a stretching surface with non-linear thermal radiation and convective boundary conditions," *Journal of Nanofluids*, vol. 8, no. 1, pp. 160–170, 2019.

[17] H. Alfvén, "Existence of electromagnetic-hydrodynamic waves," *Nature*, vol. 150, no. 3805, pp. 405-406, 1942.

[18] E. M. Sparrow and R. D. Cess, "The effect of a magnetic field on free convection heat transfer," *International Journal of Heat and Mass Transfer*, vol. 3, no. 4, pp. 267–274, 1961.

[19] O. D. Makinde and A. Aziz, "Boundary layer flow of a nanofluid past a stretching sheet with a convective boundary condition," *International Journal of Thermal Sciences*, vol. 50, no. 7, pp. 1326–1332, 2011.

[20] F. M. Hady, F. S. Ibrahim, S. M. Abdel-Gaied, and M. R. Eid, "Radiation effect on viscous flow of a nanofluid and heat transfer over a nonlinearly stretching sheet," *Nanoscale Research Letters*, vol. 7, no. 1, 2012.

[21] D. Pal, G. Mandal, and K. Vajravelu, "*MHD* convection–dissipation heat transfer over a non-linear stretching and shrinking sheets in nanofluids with thermal radiation," *International Journal of Heat and Mass Transfer*, vol. 65, pp. 481–490, 2013.

[22] I. Anwar, A. Rehaman, Z. Ismail, Z. Md. Salleh, and S. Shafie, "Chemical reaction and uniform heat generation or absorption effects on *MHD* stagnation-point flow of a nanofluid over a porous sheet," *World Applied Sciences Journal*, vol. 24, no. 10, p. 1390, 2013.

[23] M. M. Rashidi, N. Vishnu Ganesh, A. Abdul Hakeem, and B. Ganga, "Buoyancy effect on *MHD* flow of nanofluid over a stretching sheet in the presence of thermal radiation," *Journal of Molecular Liquids*, vol. 198, pp. 234–238, 2014.

[24] S. Das, R. N. Jana, and O. D. Makinde, "Magnetohydrodynamic mixed convective slip flow over an inclined porous plate with viscous dissipation and joule heating," *Alexandria Engineering Journal*, vol. 54, no. 2, pp. 251–261, 2015.

[25] S. P. A. Devi and S. S. U. Devi, "Numerical investigation of hydromagnetic hybrid Cu-Al_2O_3/water nanofluid flow over a permeable stretching sheet with suction," *International Journal of Nonlinear Sciences and Numerical Stimulation*, vol. 17, no. 5, pp. 249–257, 2016.

[26] R. Kandasamy, R. Mohammad, N. A. B. M. Zailani, and N. F. B. Jaafar, "Nanoparticle shapes on squeezed *MHD* nanofluid flow over a porous sensor surface," *Journal of Molecular Liquids*, vol. 233, pp. 156–165, 2017.

[27] S. S. Ghadikolaei, M. Yassari, H. Sadeghi, K. Hosseinzadeh, and D. D. Ganji, "Investigation on thermophysical properties of TiO_2–Cu/H_2O hybrid nanofluid transport dependent on shape factor in *MHD* stagnation point flow," *Powder Technology*, vol. 322, pp. 428–438, 2017.

[28] M. Sheikholeslami and M. Shamlooei, "Magnetic source influence on nanofluid flow in porous medium considering shape factor effect," *Physics Letters A*, vol. 381, no. 36, pp. 3071–3078, 2017.

[29] H. R. Ashorynejad and A. Shahriari, "MHD natural convection of hybrid nanofluid in an open wavy cavity," *Results in Physics*, vol. 9, pp. 440–455, 2018.

[30] S. Choudhary and V. K. Jarwal, "Magnetized nanofluid flow over a stretching sheet due to chemical reaction and non-linear thermal radiation with Navier slip and convective heating," *Journal of Rajasthan Academy of Physical Sciences*, vol. 19, no. 3and4, pp. 225–244, 2020.

[31] S. M. Atif, A. Kamran, and S. Shah, "MHD micropolar nanofluid with non-Fourier and non-Fick's law," *International Communications in Heat and Mass Transfer*, vol. 122, 2021.

[32] S. Choudhary and N. Chand, "Magnetohydrodynamic flow and heat transfer analysis on ethylene glycol based nano fluid over a vertical permeable circular cylinder with joule heating

and radiation," *Journal of Nanofluids*, vol. 11, no. 5, pp. 664–674, 2022.

[33] V. K. Jarwal, S. Choudhary, and S. Sinha, "Mixed convection boundary layer nanofluid flow over an inclined stretching cylinder with thermal radiation," *International Journal of Development Research*, vol. 13, no. 3, pp. 61935–61944, 2023.

[34] C. M. Mohana and B. Rushi Kumar, "Shape effects of Darcy–Forchheimer unsteady three-dimensional CdTe-C/H2O hybrid nanofluid flow over a stretching sheet with convective heat transfer," *Physics of Fluids*, vol. 35, no. 9, 2023.

[35] C. M. Mohana and B. R. Kumar, "Nanoparticle shape effects on hydromagnetic flow of Cu-water nanofluid over a nonlinear stretching sheet in a porous medium with heat source, thermal radiation, and Joule heating," *ZAMM- Journal of Applied Mathematics and Mechanics/Zeitschrift für Angewandte Mathematik und Mechanik*, vol. 104, no. 1, 2024.

[36] C. M. Mohana and B. R. Kumar, "Nanoparticle shape effects on MHD Cu–water nanofluid flow over a stretching sheet with thermal radiation and heat source/sink," *International Journal of Modern Physics B*, vol. 24, 2024.

[37] V. M. Falkner and S. W. Skan, "Some approximate solutions of the boundary-layer equations," *Philosophical Magazine*, vol. 12, pp. 865–896, 1931.

[38] A. Ishak, R. Nazar, and I. Pop, "Falkner-Skan equation for flow past a moving wedge with suction or injection," *Journal of Applied Mathematics and Computing*, vol. 25, no. 1-2, pp. 67–83, 2007.

[39] N. A. Yacob, A. Ishak, and I. Pop, "Falkner-Skan problem for a static or moving wedge in nanofluids," *International Journal of Thermal Sciences*, vol. 50, no. 2, pp. 133–139, 2011.

[40] H. Tamim, S. Dinarvand, R. Hosseini, and I. Pop, "*MHD* mixed convection stagnation-point flow of a nanofluid over a vertical permeable surface: a comprehensive report of dual solutions," *Heat and Mass Transfer*, vol. 50, no. 5, pp. 639–650, 2013.

[41] S. Nadeem, S. Ahmad, and N. Muhammad, "Computational study of Falkner-Skan problem for a static and moving wedge," *Sensors and Actuators B: Chemical*, vol. 263, pp. 69–76, 2018.

[42] S. A. Gaffar, V. R. Prasad, B. R. Kumar, and O. A. Beg, "Computational modelling and solutions for mixed convection boundary layer flows of nanofluid from a non-isothermal wedge," *Journal of Nanofluids*, vol. 7, no. 5, pp. 1024–1032, 2018.

[43] P. Sudhagar, P. K. Kameswaran, and B. R. Kumar, "Non-Darcy effects on mixed convective nanofluid over a wedge in a porous medium," *Journal of Porous Media*, vol. 21, no. 9, pp. 781–791, 2018.

[44] S. Dinarvand, M. N. Rostami, and I. Pop, "A novel hybridity model for TiO_2-CuO/water hybrid nanofluid flow over a static/moving wedge or corner," *Scientific Reports*, vol. 9, no. 1, 2019.

[45] G. Kumaran, R. Sivaraj, A. Subramanyam Reddy, B. Rushi Kumar, and V. Ramachandra Prasad, "Hydromagnetic forced convective flow of Carreau nanofluid over a wedge/plate/stagnation of the plate," *The European Physical Journal- Special Topics*, vol. 228, no. 12, pp. 2647–2659, 2019.

[46] A. Bibi and H. Xu, "Peristaltic channel flow and heat transfer of Carreau magneto hybrid nanofluid in the presence of homogeneous/heterogeneous reactions," *Scientific Reports*, vol. 10, no. 1, 2020.

[47] S. K. Rawat, S. Negi, H. Upreti, and M. Kumar, "A non-fourier's and non-fick's approach to study MHD mixed convective copper water nanofluid flow over flat plate

subjected to convective heating and zero wall mass flux condition," *International Journal of Algorithms, Computing and Mathematics*, vol. 7, no. 6, 2021.

[48] B. Mahanthesh, S. A. Shehzad, T. Ambreen, and S. U. Khan, "Significance of Joule heating and viscous heating on heat transport of MoS_2–Ag hybrid nanofluid past an isothermal wedge," *Journal of Thermal Analysis and Calorimetry*, vol. 143, no. 2, pp. 1221–1229, 2021.

[49] N. Kakar, A. Khalid, A. S. Al-Johani, N. Alshammari, and I. Khan, "Melting heat transfer of a magnetized water-based hybrid nanofluid flow past over a stretching/shrinking wedge," *Case Studies in Thermal Engineering*, vol. 30, 2022.

[50] M. M. Bhatti, H. F. Oztop, and R. Ellahi, "Study of the magnetized hybrid nanofluid flow through a flat Elastic surface with applications in solar energy," *Materials*, vol. 15, no. 21, p. 7507, 2022.

[51] M. Yaseen, S. K. Rawat, and M. Kumar, "Falkner–Skan problem for a stretching or shrinking wedge with nanoparticle aggregation," *Journal of Heat Transfer*, vol. 144, no. 10, 2022.

[52] S. Kumar Rawat, M. Yaseen, U. Khan et al., "Insight into the significance of nanoparticle aggregation and non-uniform heat source/sink on titania–ethylene glycol nanofluid flow over a wedge," *Arabian Journal of Chemistry*, vol. 16, no. 7, 2023.

[53] S. Kumar, S. Choudhary, and A. Sharma, "MHD Williamson nano fluid past a moving permeable wedge with non-linear radiation and chemical reaction effects using Buongiorno model," *Industrial Engineering Journal*, vol. 16, no. 12, pp. 1672–1697, 2023.

[54] Y. Bing Kho, R. Jusoh, M. Zuki Salleh, M. Hisyam Ariff, and N. Zainuddin, "Magnetohydrodynamics flow of Ag-TiO_2 hybrid nanofluid over a permeable wedge with thermal radiation and viscous dissipation," *Journal of Magnetism and Magnetic Materials*, vol. 565, 2023.

[55] R. K. Tiwari and M. K. Das, "Heat transfer augmentation in a two-sided lid-driven differentially heated square cavity utilizing nanofluids," *International Journal of Heat and Mass Transfer*, vol. 50, no. 9-10, pp. 2002–2018, 2007.

[56] F. M. White, *Viscous Fluid Flow*, McGraw-Hill, New York, NY, USA, 3rd edition, 2006.